

Online Research @ Cardiff

This is an Open Access document downloaded from ORCA, Cardiff University's institutional repository: <https://orca.cardiff.ac.uk/id/eprint/59557/>

This is the author's version of a work that was submitted to / accepted for publication.

Citation for final published version:

Fagereng, Ake ORCID: <https://orcid.org/0000-0001-6335-8534> 2014.
Significant shortening by pressure solution creep in the Dwyka diamictite, Cape Fold Belt, South Africa. *Journal of African Earth Sciences* 97 , pp. 9-18.
10.1016/j.jafrearsci.2014.04.022 file

Publishers page: <http://dx.doi.org/10.1016/j.jafrearsci.2014.04.022>
<<http://dx.doi.org/10.1016/j.jafrearsci.2014.04.022>>

Please note:

Changes made as a result of publishing processes such as copy-editing, formatting and page numbers may not be reflected in this version. For the definitive version of this publication, please refer to the published source. You are advised to consult the publisher's version if you wish to cite this paper.

This version is being made available in accordance with publisher policies.

See

<http://orca.cf.ac.uk/policies.html> for usage policies. Copyright and moral rights for publications made available in ORCA are retained by the copyright holders.



Å. Fagereng: Pressure solution cleavage in Dwyka diamictite

1 Significant shortening by pressure solution creep in the Dwyka
2 diamictite, Cape Fold Belt, South Africa

3

4 Åke Fagereng

5

6 Department of Geological Sciences, University of Cape Town, Rondebosch 7701, South Africa

7

8 Corresponding author: e-mail: ake.fagereng@uct.ac.za

9

10

11

12

13

14

15

16

17

18

19

20

21

22

23 **Abstract**

24

25 The Dwyka diamictite preserves a record of horizontal shortening related to the development of
26 the Cape Fold Belt at subgreenschist conditions. This shortening was accommodated by folding
27 and thrust faulting, but pressure solution may also have contributed significantly to bulk
28 deformation. Cleavage within the Dwyka group is, in the studied part of the Karoo Basin,
29 subvertical to moderately south dipping, and approximately axial planar to regional folds. The
30 cleavage is anastomosing, leading to the development of ‘tombstone cleavage’, and defined
31 microscopically by thin seams of fine grained dark material. X-ray diffraction analyses show that
32 the diamictite matrix is made up of quartz, feldspars, muscovite and chlorite. Element maps
33 further indicate that the cleavage is defined predominantly by phyllosilicates and minor oxides,
34 implying that it is made up of relatively insoluble material and hydrothermal alteration products.
35 Overall, the cleavage therefore formed by dissolution and removal of mobile elements. This
36 indicates that pressure solution likely accommodated a significant component of shortening
37 during the Cape Orogeny, and provides an example of low temperature cleavage development
38 during orogenesis.

39

40

41

42

43

44

45

46

47 **Introduction**

48 On short time scales, the upper crust deforms by high strain rate brittle deformation (Byerlee,
49 1978, Sibson, 1983; Kohlstedt et al., 1995); whereas on longer time scales, the upper crust can
50 deform ductilely at slower strain rates by viscous deformation controlled by stress-driven, fluid-
51 assisted, diffusive mass transfer (Durney, 1972; McClay, 1977; Rutter, 1983; Gratier et al.,
52 2013). These deformation styles may coexist spatially, as illustrated by coeval folds and faults in
53 foreland fold-and-thrust belts (e.g. Suppe, 1983; Mitra, 1990; Mantero et al., 2011). During such
54 coeval brittle-viscous deformation, brittle deformation is envisaged to occur episodically at fast
55 strain rates, between longer episodes dominated by continuous viscous deformation (e.g. Gratier
56 and Gamond, 1990; Gratier et al., 2013).

57

58 The Cape Fold Belt records ductile behaviour of rocks deformed in the upper crust (du Toit,
59 1937; de Wit and Ransome, 1992; Fagereng, 2012), and represents a natural laboratory for the
60 contribution of pressure solution to large scale folding. The Dwyka Group diamictite, at the base
61 of the Karoo Supergroup which fills the foreland basin of the Cape Fold Belt, has a particularly
62 striking subvertical to steeply inclined cleavage, here argued to result from pressure solution, the
63 dissolution of material by grain boundary, fluid-assisted, stress-driven diffusion. The purpose of
64 this paper is to describe the spaced solution cleavage in the Dwyka Group in detail, and discuss
65 its formation and role in the development of the Cape Fold Belt, with implications for pressure
66 solution in fold-and-thrust belts in general.

67

68

69 **Geological setting**

70

71 The Cape Fold Belt formed along the southern margin of Gondwana (du Toit, 1937; de Wit and
72 Ransome, 1992; Hälbich, 1992), in response to compression and accretion in a fold belt that can
73 be traced from the Sierra de la Ventana in Argentina, through South Africa, to the Trans-
74 Antarctic Mountains (du Toit, 1937; de Wit and Ransome, 1992; Dalziel et al., 2000). In a South
75 African context, deformation related to this fold belt affects clastic sedimentary rocks of the
76 Ordovician to Early Carboniferous Cape Supergroup, and the Late Carboniferous to Middle
77 Jurassic Karoo Supergroup. The Cape Fold Belt is divided into a ‘western arm’, with a north-
78 south structural trend, and a ‘southern arm’, where structures generally strike east-west (Figure
79 1a). The two arms meet northeast of Cape Town, in the syntaxis of the fold belt. The southern
80 arm, in which the current study area is located, is characterised by north-verging folds and
81 reverse faults recording predominantly north-south shortening (Hälbich, 1993; Paton *et al.*, 2006;
82 Lindeque *et al.*, 2011)(Figure 1b). Cross-section reconstructions and field observations indicate
83 at least two episodes of tectonic reactivation affecting rocks of the Cape and Karoo Supergroups:
84 (1) formation of the Cape Fold Belt involved positive inversion of normal faults, developed
85 before and during deposition of the Cape Supergroup in an intra-continental clastic margin; and
86 (2) negative inversion of Cape Fold Belt related structures during the break-up of Gondwana
87 (Paton *et al.*, 2006).

88

89 The Cape Fold Belt is generally thought to reflect shallow angle subduction of the paleo-Pacific
90 towards the north underneath Gondwana (Lock, 1980; de Wit and Ransome, 1992; Hälbich,
91 1992, 1993). Alternative tectonic models for the collision, however, include a transpressional

92 setting (Tankard *et al.*, 2009) and subduction towards the south, culminating in collision with a
93 crustal block now part of South America (Lindeque *et al.*, 2011). The Karoo Basin is considered
94 to be a retro-arc foreland basin, which formed in response to the tectonic load caused by
95 mountain building in the Cape Fold Belt (Catuneanu *et al.*, 1998, 2005; Catuneanu, 2004).
96 Tankard *et al.* (2009) have, however, suggested that the Cape Fold Belt initiated only in the
97 Triassic, after the late Carboniferous initiation of sedimentation in the Karoo Basin. In their
98 model, Karoo subsidence was facilitated by crustal-scale faults and not associated with a
99 foreland basin. Irrespective of large-scale tectonic model, the Cape Fold Belt and Karoo Basin
100 developed with some overlap in time, and the Karoo Basin was filled by sediments derived by
101 erosion of the adjacent mountains of the Cape Fold Belt (e.g. Catuneanu *et al.*, 2005 and
102 references therein). The sediments of the Karoo Basin, in areas adjacent to the Cape Fold Belt,
103 were then also deformed as a result of regional compression.

104
105 The Dwyka Group is the oldest sedimentary unit of the Karoo Supergroup, and reflects a
106 Gondwana glaciation from 302 to 290 Ma (Bangert *et al.*, 1999). The Dwyka Group is present
107 over large areas of southern Africa, and contains both continental and marine facies (Visser,
108 1987, 1997; Visser *et al.*, 1997). Here, focus is on deformation of the Dwyka in an area adjacent
109 to the Cape Fold Belt, and therefore in the foredeep marine facies as discussed by Catuneanu
110 (2004). In the foredeep of the proposed retro-arc foreland Karoo Basin, the Dwyka Group
111 comprises four upward-fining sequences of massive to stratified diamictites reaching up to 800
112 m in total thickness (Visser, 1997). The diamictites are composed of a silt-dominated matrix with
113 dropstones of variable size, shape, and composition, derived from floating ice. The strata are
114 uniform and laterally continuous, indicating deposition from suspension in a low energy

115 environment (Visser, 1987). In places, there is evidence for re-sedimentation by debris flow
116 (Visser, 1997), and, in general, bedding planes are not recognizable in outcrop, because of re-
117 sedimentation and/or bedding thicknesses exceeding the size of the outcrop.

118

119 In the study area, the Dwyka Group is separated from the underlying Cape Supergroup by an
120 unconformity that represents approximately 30 million years of missing rock record, inferred to
121 reflect a period of regional uplift related to collision during the mid-Carboniferous assembly of
122 Pangea (Catuneanu *et al.*, 2005). The diamictites are overlain by the Prince Albert Formation,
123 which is the lowest part of the post-glacial Eccca Group. The transition from the Dwyka to the
124 Eccca Group is reflected in a gradual contact between mudstones with and without dropstones
125 respectively. The Prince Albert Formation is interpreted as a marine mudstone sequence, with
126 sediments derived from the growing Cape Fold Belt mountains to the south (Catuneanu *et al.*,
127 1998). Structure in the study area, which is in the frontal range of the Cape Fold Belt (Figure 1),
128 represents a northward transition from north-verging, open to tight folds, to upright, open folds.
129 Further north, the strata are approximately horizontal. Cleavage is generally axial planar, i.e.
130 subvertical to moderately south dipping (Figure 2a,b). Horizontal pencil lineation (formed at the
131 intersection between cleavage and bedding) attest to subhorizontal fold hinge lines. Fluid
132 inclusions imply temperatures less than 200°C during deformation in this area (Egle *et al.*, 1998).
133

134 **Field and microstructural observations**

135

136 In the Laingsburg region, fold geometry changes from north-verging, moderately inclined, tight
137 to open folds with locally overturned limbs (Figures 1c, 2a), to upright, open folds (Figures 1b,

138 2b). The former occurs in Cape Supergroup rocks, and the Dwyka and Eccca Group rocks that
139 crop out adjacent to the northernmost exposures of the Cape Supergroup, whereas upright
140 folding becomes predominant further north (Figure 1b). Cleavage is generally axial planar, and
141 as a result, cleavage in the Dwyka varies in orientation from steeply to moderately inclined,
142 reflecting a variation in fold inclination (Figure 2c). Strike of cleavage planes, however, is
143 relatively uniform and E-W to WNW-ESE.

144
145 At outcrop scale, cleavage in the Dwyka is anastomosing and curvi-planar. Because cleavage
146 planes represent planes of relative weakness, mechanical erosion leads to formation of so-called
147 ‘tombstone cleavage’, where blocks separated by anastomosing cleavage surfaces dominate the
148 surface exposure of the Dwyka (Figure 3a,b). The long axes of these ‘tombstones’ are parallel to
149 the average dip direction of the anastomosing cleavage planes, and therefore moderately to
150 steeply plunging (Figure 3a,b,c). The size of the tombstones (as measured by the length of their
151 long axes), increases as a function of the largest dropstone contained within them (Figure 4). The
152 Dwyka diamictites also preserve fractured dropstones, where tensile fractures are constrained to
153 the dropstones, and oriented approximately perpendicular to cleavage (Figure 3c).

154
155 At the micro-scale, the cleavage is also anastomosing and curvi-planar (Figure 5a-c). Cleavage
156 surfaces are defined by fine-grained black material, which forms wavy surfaces through the
157 matrix, and that wrap around dropstones and larger clasts in the matrix (Figure 5a,b). A near-
158 perpendicular angular relationship between cleavage and tensile fractures within dropstones is
159 apparent also on the micro-scale (Figure 5c). Because the cleavage does not cut through
160 dropstones, but curves around them, the cleavage spacing is to a first order controlled by

161 dropstone size (Figure 5a). On the other hand, very small spacing between cleavage surfaces
162 occurs at the edge of some dropstones (Figure 5b). Cleavage spacing thereby varies from < 10
163 μm to several hundred μm . Dropstones, particularly those composed of quartz, commonly appear
164 as shortened or dissolved along the cleavage surfaces (Figure 5a). As a consequence, dropstones
165 have a general qualitative shape-preferred orientation subparallel to the cleavage seams (Figure
166 5a). Overall, the cleavage has all the characteristics of a pressure solution cleavage: (1) it is
167 defined by dark, very fine grained seams; (2) cleavage intensity increases in what would be
168 higher stress areas, such as areas where dropstones are near or in contact with each other (Figure
169 5b); (3) cleavage is more developed in finer grained material, i.e. the matrix, and not in coarse
170 grained dropstones; (4) where the cleavage is in contact with dropstones, the dropstones are
171 commonly cut off (inferred as dissolved) along the cleavage surface (Figure 5a-c); and (5) the
172 cleavage is perpendicular to tensile fractures, as expected if dissolution cleavage and tensile
173 fractured formed in the same stress field.

174

175 **Composition of cleavage surfaces**

176

177 X-Ray diffraction (XRD) and electron microprobe (EMP) analyses have been applied to address
178 the composition of the fine-grained cleavage surfaces in the Dwyka diamictites. XRD was
179 performed on powdered samples of matrix material, using a Phillips XRD system equipped with
180 a PW 3830/40 generator, a PW 3710 MPD diffractometer control, and Xpert data collector and
181 identity software, housed in the Department of Geological Sciences, University of Cape Town.
182 Measurement conditions were 40 kV, 25 mA, CuK_α radiation with 1° slits, and samples were
183 scanned from 3 to $70^\circ 2\theta$ with a step size of $0.025^\circ 2\theta$ and counting time of 0.4 s. Element maps

184 were measured using a JEOL JXA-8100 Electron Probe Microanalyser, housed in the
185 Department of Geological Sciences, University of Cape Town. Analyses were performed with
186 beam conditions of 15 kV, 18.5 nA, 12 ms dwell time, and spot size of 1 μm .

187
188 The XRD patterns are similar for all the exposed cycles of the Dwyka group in the field area
189 (Figure 6). The peaks in the spectra can be accounted for by quartz, feldspar (albite \pm anorthite
190 and microcline), illite-muscovite, and chlorite. There may be a number of types of white mica
191 here grouped and described as illite-muscovite, but detailed clay mineralogy is beyond the scope
192 of this contribution. Based on relative intensity of XRD peaks, quartz is by far the most abundant
193 mineral in the Dwyka matrix material, which is also apparent based on optical petrography (Fig.
194 5). Phyllosilicates are relatively minor, but present in all samples, and with chlorite appearing
195 more abundant than white mica. There is no significant mineralogical difference between the
196 matrix materials of the different Dwyka cycles, indicating that grain size is the only lithological
197 parameter that varies significantly within the matrix of the Dwyka.

198
199 The element map in Figure 7 shows an area adjacent to a small, boudinaged, quartz clast. In this
200 sample, clasts are elongate subparallel to cleavage surfaces. In an electron backscatter image, the
201 cleavage planes appear relatively bright, compared to clasts of quartz. The edges of the quartz
202 clasts are depleted in Si, in line with an interpretation of dissolution along grain boundaries.
203 Quartz grain boundaries parallel to the cleavage are enriched in Fe and K, consistent with Fe-
204 oxides and phyllosilicates. The cleavage seams have low Si concentrations, and show elevated
205 concentrations of K, Al, and Fe, relative to the surrounding material. Ca is rare throughout the
206 sample, and Ti was under the detection limit of the instrument (and therefore not displayed).

207
208 An area of high cleavage intensity was mapped and displayed in Fig. 8. Again, cleavage seams
209 stand out in an electron backscatter image as brighter (greater number of backscattered electrons)
210 than surrounding material. The seams are depleted in Si, marginally elevated in Al, and
211 significantly enriched in K and Fe, compared to the rest of the sample. Feldspar (in the lower left
212 corner) is partially replaced by K and minor Fe, consistent with hydration reactions locally
213 forming phyllosilicates.

214

215 **Discussion**

216 *Process and conditions of cleavage formation*

217 The microstructure of the folded and cleaved Dwyka diamictites is typical of rocks deformed by
218 pressure solution creep, with seams of insoluble material defining the cleavage planes.
219 Specifically, the pressure solution cleavage in the Dwyka appears defined by phyllosilicates and
220 Fe-oxides. Cleavage defined by dark, fine grained seams of Fe-oxides and phyllosilicates are
221 also observed in other rocks inferred to have deformed by pressure solution creep, for example in
222 the Otago Schist (Fagereng and Cooper, 2010), shales of the Shimanto Complex (Kawabata et
223 al., 2007), along the San Andreas fault (Gratier *et al.*, 2011), and in the Willard thrust system,
224 Utah (Yonkee et al., 2013). The pressure solution cleavage spacing is strongly affected by the
225 size of competent dropstones within the Dwyka diamictites. On the outcrop scale, this leads to an
226 anastomosing cleavage network separating less strongly cleaved lenses, appearing as
227 ‘tombstones’ after weathering (Fig. 3a,b). The size of these less deformed lenses is a function of
228 the dimensions of the largest dropstone each contains (Fig. 4). On the microscale, lithic, quartz
229 and feldspar clasts in the matrix, which likely represent small dropstones, are not cleaved, and

230 pressure solution cleavage wraps around the clasts (Fig. 5a-c). Cleavage intensity appears highest
231 at clast boundaries and between closely spaced clasts (Fig. 5a,b), which are areas of inferred
232 greater normal stress. This observation implies that cleavage seams developed preferentially in
233 high stress areas, as expected for pressure solution cleavage (e.g. Durney, 1972).

234
235 Craddock *et al.* (2007) quantified the stress-strain field of cleavage formation in the Dwyka
236 based on calcite twin fabric in syn-cleavage veins (subhorizontal calcite-filled extension
237 fractures within clasts, as in Fig. 3c) and a limestone clast. They calculated a south-trending
238 (181° average), subhorizontal least stretch, with a magnitude of -4.8% , in response to an
239 average differential stress of 46 MPa. They also obtained a vertical intermediate strain axis, and
240 an east-west trending, horizontal, greatest stretch. In the region where they took their samples
241 and measurements, the folding in the Dwyka is approximately upright, with a subvertical
242 cleavage (Fig. 2b), so that the least stretch is cleavage-normal and subhorizontal. Considering a
243 larger area, cleavage is subvertical to moderately south-dipping (Fig. 2c), implying a
244 subhorizontal to moderately northward-plunging least stretch. This is consistent with north-south
245 shortening and pure shear in the Karoo Basin north of the Cape Fold Belt, and requires a
246 component of top-to-the-north simple shear in the frontal range of the fold belt, consistent with
247 northward movement of thrust sheets.

248
249 Consistent, subhorizontal, extension fracture orientations within dropstones (Craddock *et al.*,
250 2007; this study), are consistent with a subvertical least compressive stress, as expected in an
251 Andersonian stress field favouring reverse faulting. These extension fractures are confined to
252 competent dropstones within the matrix, and their consistent orientation implies minor rotation

253 of dropstones, at least around a horizontal axis, during deformation involving coeval folding,
254 fracturing, and cleavage formation. The presence of subhorizontal tensile fractures, by itself,
255 implies that at least locally and transiently, fluid pressure must have exceeded the lithostatic
256 stress (Secor, 1965).

257

258 ***Kinetics of pressure solution creep***

259 The importance of pressure solution in the development of the Cape Fold Belt depends on its
260 kinetics; in other words whether it could achieve sufficiently high strain rates to be of
261 significance to the overall deformation. Gratier *et al.* (2009) derived an empirical flow law for
262 pressure solution creep limited by diffusion, of the form:

$$263 \quad \dot{\epsilon} = \frac{8DwcV_s(e^{3\Delta\sigma_n V_s / RT} - 1)}{d^3} \quad (1)$$

264 where D is the diffusion constant along the stressed interface, w is the thickness of the fluid
265 phase within which diffusion occurs, c is the solubility of the dissolved solid, V_s is the molar
266 volume of the stressed solid, $\Delta\sigma_n$ is the driving stress, inferred to be the difference in normal
267 stress between the stressed surface and a low stress deposition site (e.g. fluid pressure in a vein),
268 R is the universal gas constant, T is temperature in Kelvin, and d is the diffusive mass transfer
269 distance.

270

271 The parameter d is either fracture spacing or grain size. In this example, grain size is likely the
272 control on mass transfer, as although veins are present locally within competent clasts, most
273 mass transfer occurred by fluid-assisted grain boundary diffusion within the less competent
274 matrix, as illustrated by cleavage development being characteristic of the matrix and not its
275 clasts. If ‘tombstones’ are indeed defined by anastomosing cleavage planes, then the observation

276 that tombstone size is controlled by drop stone size (Fig. 4), implies that grain size and cleavage
277 spacing are related. This is not surprising, and implies that cleavage spacing is also a measure of
278 d , as the transport distance from precipitation to dissolution is constrained by the distance to a
279 dissolution seam.

280

281 Quartz is the main mineral dissolved along the dissolution seams, and is also a major component
282 of the matrix (Figs. 6,7,8). The molar volume of quartz is $2.2 \times 10^{-5} \text{ m}^3 \text{ mol}^{-1}$. According to the
283 empirical quartz solubility calculation of Rimstidt (1997), solubility of quartz in water at 200°C
284 is approximately $4.3 \times 10^{-3} \text{ mol m}^{-3}$, and goes up to $7.2 \times 10^{-3} \text{ mol m}^{-3}$ at 250°C (upper boundary
285 of fluid temperature in the foothills of the Cape Fold Belt, Egle *et al.*, 1998). The factors D and w
286 are poorly constrained, but based on pressure solution experiments by Gratier *et al.* (2009) and
287 quartz diffusion data presented by Brady (1995), D is approximately $1 \times 10^{-10} \text{ m}^2 \text{ s}^{-1}$ for the 200 -
288 350°C range, whereas w is between 2 and 10 nm (Gratier *et al.*, 2009). Like Gratier *et al.* (2009,
289 2011) I therefore use an average value for the product $Dw = 5.7 \times 10^{-19} \text{ m}^3 \text{ s}^{-1}$. A differential
290 stress $\Delta\sigma_n$ of 46 MPa, measured by Craddock (2007) based on vein calcite is taken as an estimate
291 for the stress difference between sites of dissolution and precipitation.

292

293 Figure 9 shows a plot of strain rate against d , contoured for temperature calculated using Eq. 1.
294 The temperature control on quartz solubility does not have a major effect on strain rate compared
295 to the potential variation in d . The factor d has a major effect arising both from inherent variation
296 in diffusive distance in heterogeneous diamictites, and from the formulation of the pressure
297 solution flow law (Eq. 1) where strain rate is inversely proportional to the cube of d . If cleavage
298 spacing, typically between $10 \mu\text{m}$ and 1 mm (Fig 5), is representative of d , then for temperatures

299 between 150 and 250°C, strain rates of 10^{-16} s^{-1} to 10^{-9} s^{-1} could be achieved. The range primarily
300 represents a variation in transport distance between Dwyka cycles with high and low proportions
301 of coarse dropstones. On the scale of orogenic strain rates, these potential strain rates achieved
302 by pressure solution are high. For d less than about 0.3 mm, a grain size relatively common in
303 the Dwyka matrix, as well as a distance comparable to cleavage spacing within this matrix (Fig.
304 5), predicted strain rate is higher than the global average of approximately $4 \times 10^{-14} \text{ s}^{-1}$ (Pfiffner
305 and Ramsay, 1982), and higher than pressure solution strain rates of $1 - 4 \times 10^{-15} \text{ s}^{-1}$ calculated
306 for thrust sheets in the southern Pyrenees (Burbank et al., 1992; Holl and Anastasio, 1993), a
307 fold-and-thrust belt deformed at comparable conditions to the Cape Fold Belt.

308

309 *Implications for interpretations of the Cape Fold Belt*

310 Discussion on strain distribution in the Cape Fold Belt (e.g. Paton et al., 2006), and
311 interpretations on the relative contributions of faulting and folding (e.g. Booth and Shone, 2002;
312 Booth, 2011), have not considered the contribution from cleavage development to overall
313 horizontal shortening. The Dwyka diamictite is folded, but also contains a subvertical pressure
314 solution cleavage contributing additional shortening. The magnitude of this shortening is
315 unknown, and difficult to estimate. Based on dropstone shape change caused by pressure
316 solution, one could qualitatively estimate shortening on the order of 5 % (Fig. 5), but this may
317 underestimate shortening by dissolution of smaller inclusions and of the matrix material.

318

319 The strain rates associated with pressure solution are capable of similar or higher deformation
320 rates to those typically associated with orogenic fold and thrust belts. Although the shortening
321 associated with the Cape Fold Belt is poorly constrained, it should therefore be noted that

322 pressure solution likely increases any current estimates. In addition, the potential strain rates
323 accommodated by pressure solution creep imply that the viscosity of the Dwyka diamictites was
324 sufficiently low for flow at strain rates typical of compressional margins. A corollary of this
325 inference is that the Dwyka, despite containing large, strong clasts, had a bulk rheology that was
326 relatively weak compared to surrounding quartzites (top of Cape Supergroup) and sandstones
327 (higher in the Karoo Supergroup), which are highly fractured and thus their bulk rheology is
328 better described by a Coulomb criterion with shear strength proportional to normal stress.

329
330 Cleavage formation and associated shape-preferred fabric in the Dwyka diamictites are
331 interpreted to have formed by pressure solution creep, and little evidence is seen for soft
332 sediment folding (although other soft sediment deformation, e.g. slumping, has been reported;
333 Visser, 1997). Although pressure solution can occur at shallow depths, the diamictites were
334 likely consolidated at the time the spaced axial planar cleavage developed. Consequently, folding
335 would have initiated after at least some burial of the Dwyka Group, but at less than the 200-
336 250°C inferred for the maximum temperature in this part of the Cape Fold Belt (Egle, 1998).

337
338 The axial planar cleavage in the Dwyka is consistent with pure shear, with a component of
339 rotation around a horizontal axis present closer to the hinterland. This is typical for fold-and-
340 thrust belts, and implies north-south shortening across the east-west trending southern arm of the
341 Cape Fold Belt. This is consistent with uniaxial shortening, and does not require a
342 transpressional component, as suggested by Tankard et al. (2009).

343

344 **Conclusions**

345

346 The Dwyka diamictite in the foreland of the Cape Fold Belt preserves an axial planar cleavage
347 defined by very fine grained phyllosilicates and minor Fe-Mg oxides, interpreted as a spaced
348 solution cleavage. The cleavage is anastomosing, with spacing controlled by the size of
349 dropstones, which vary in the largest dimension from centimetres or less to more than a metre.
350 Because the cleavage wraps around these dropstones, cleavage spacing and inferred strain
351 intensity is highly variable, as reflected by the anastomosing nature of the cleavage.

352

353 Based on a pressure solution flow law, the strain rate that could be achieved by diffusive mass
354 transfer in the Dwyka is sufficient to account for typical strain rates of 10^{-14} - 10^{-15} s⁻¹ as inferred
355 in other fold-and-thrust belts, or faster in finer grained Dwyka cycles. The potentially high strain
356 rates imply that the Dwyka Group may have been a relatively weak layer within the folding
357 sequence during formation of the Cape Fold Belt. Considering the dense cleavage spacing
358 observed particularly in fine grained intervals, it is likely that the creation of a subvertical
359 pressure solution cleavage contributed significantly to horizontal shortening in this area.

360

361

362 **Acknowledgments**

363 A UCT Research Development Grant and NRF Incentive Funding for Rated Researchers have
364 provided funding for work on deformation mechanisms and deformation localization. I thank
365 Carly Faber for assistance with fieldwork and development of the ideas presented in the
366 manuscript, and I am grateful to Christel Tinguely and Tanya Dreyer for their efforts with the

367 microprobe and XRD analyses. Two anonymous reviewers provided comments that improved
368 the final paper.

369

370 **References**

371 Bangert, B., Stollhofen, H., Lorenz, V. and Armstrong, R. (1999). The Geochronology and
372 significance of ash-fall tuffs in the glaciogenic Carboniferous-Permian Dwyka Group of
373 Namibia and South Africa. *Journal of African Earth Sciences*, **29**, 33-49.

374 Booth, P.W.K. (2011). Stratigraphic, structural and tectonic enigmas associated with the Cape
375 Fold Belt: challenges for future research. *South African Journal of Geology*, **114**, 235-248.

376 Booth, P.W.K. and Shone, R.W. (2002). A review of thrust faulting in the Eastern Cape Fold
377 Belt, South Africa, and the implications for current lithostratigraphic interpretation of the
378 Cape Supergroup. *Journal of African Earth Sciences*, **34**, 179-190.

379 Brady, J.B. (1995). Diffusion data for silicate minerals, glasses, and liquids. *Mineral Physics and*
380 *Crystallography: A Handbook of Physical Constants*. American Geophysical Union,
381 Reference Shelf vol. 2, pp. 269-290.

382 Burbank, D.W., Verges, J., Muñoz, J.A. and Bentham, P. (1992). Coeval hindward- and forward-
383 imbricating thrusting in the central southern Pyrenees, Spain: timing and rates of
384 shortening and deposition. *Bulletin of the Geological Society of America*, **104**, 3-17.

385 Byerlee, J. D. (1978). Friction of rocks. *Pure and Applied Geophysics*, **116**, 615-626.

386 Catuneanu, O. (2004). Basement control on flexural profiles and the distribution of foreland
387 facies: the Dwyka Group of the Karoo Basin, South Africa. *Geology*, **32**, 517-520.

- 388 Catuneanu, O., Hancox, P.J. and Rubidge, B.S. (1998). Reciprocal flexural behaviour and
389 contrasting stratigraphies: a new basin development model for the Karoo retroarc foreland
390 system, South Africa. *Basin Research*, **10**, 417-439.
- 391 Catuneanu, O., Wopfner, H., Eriksson, P.G., Cairncross, B., Rubidge, B.S., Smith, R.M.H. and
392 Hancox, P.J. (2005). The Karoo basins of south-central Africa. *Journal of African Earth
393 Sciences*, **43**, 211-253.
- 394 Craddock, J.P., McKiernan, A.W. and de Wit, M.J. (2007). Calcite twin analysis in syntectonic
395 calcite, Cape Fold Belt, South Africa: Implications for fold and cleavage formation within
396 a shallow thrust front. *Journal of Structural Geology*, **29**, 1100-1113.
- 397 Dalziel, I.W.D., Lawver, L.A. and Murphy, J.B. (2000). Plumes, orogenesis, and
398 supercontinental fragmentation. *Earth and Planetary Science Letters*, **178**, 1-11.
- 399 de Wit, M.J. and Ransome, I.G.D. (1992). Regional inversion tectonics along the southern
400 margin of Gondwana. In M.J. de Wit and I.G.D. Ransome (Editors), *Inversion Tectonics of
401 the Cape Fold Belt, Karoo and Cretaceous Basins of Southern Africa*. Balkema, Rotterdam,
402 pp. 15-22.
- 403 Durney, D. W. (1972). Solution-transfer, an important geological deformation mechanism.
404 *Nature*, **235**, 315-317.
- 405 du Toit, A.L. (1937). *Our Wandering Continents*. Oliver and Boyd, Edinburgh.
- 406 Egle, S., de Wit, M.J. and Hoernes, S. (1998). Gondwana fluids and subsurface palaeohydrology
407 of the Cape Fold Belt and the Karoo Basin, South Africa. *Journal of African Earth
408 Sciences*, **27**, 63-64.
- 409 Fagereng, Å. (2012). A note on folding mechanisms in the Cape Fold Belt, South Africa. *South
410 African Journal of Geology*, **115**, 137-144.

- 411 Fagereng, Å. and Cooper, A.F. (2010). The metamorphic history of rocks buried, accreted and
412 exhumed in an accretionary prism: an example from the Otago Schist, New Zealand.
413 *Journal of Metamorphic Geology*, **28**, 935-954.
- 414 Gratier, J.P. and Gamond, J.F. (1990). Transition between seismic and aseismic deformation in
415 the upper crust. In R.J. Knipe and E.H. Rutter (Editors), *Deformation Mechanisms,*
416 *Rheology and Tectonics*. Geological Society, London, *Special Publication*, **54**, 461-473.
- 417 Gratier, J.P., Guiguet, R., Renard, F., Jenatton, L. and Bernard, D. (2009). A pressure solution
418 creep law for quartz from indentation experiments. *Journal of Geophysical Research-Solid*
419 *Earth*, **114**, doi:10.1029/2008JB005652.
- 420 Gratier, J.P., Richard, J., Renard, F., Mittempergher, S., Doan, M.-L., Di Toro, G., Hadizadeh, J.
421 and Boullier, A.-M. (2011). Aseismic sliding of active faults by pressure solution creep:
422 Evidence from the San Andreas Fault Observatory at Depth. *Geology*, **39**, 1131-1134.
- 423 Gratier, J.P., Dysthe, D. and Renard, F. (2013). The role of pressure solution creep in the
424 ductility of the Earth's upper crust. *Advances in Geophysics*, **54**, doi:10.1016/B978-0-12-
425 380940-7.00002-0.
- 426 Hålbich, I.W., 1992. The Cape Fold Belt orogeny: State of the art 1970s-1980s. In M.J. de Wit
427 and I.G.D. Ransome (Editors), *Inversion Tectonics of the Cape Fold Belt, Karoo and*
428 *Cretaceous Basins of Southern Africa*. Balkema, Rotterdam, pp. 141-158.
- 429 Hålbich, I.W., 1993. The Cape Fold Belt-Agulhas Bank transect across Gondwana Suture,
430 Southern Africa. *Global Geoscience Transect*, **9**, American Geophysical Union,
431 Washington, 18 pp.
- 432 Holl, J.E., Anastasio, D.J., 1993. Paleomagnetically derived folding rates southern Pyrenees,
433 Spain. *Geology*, **21**, 271-274.

- 434 Kawabata, K., Tanaka, H., Kimura, G., 2007. Mass transfer and pressure solution in deformed
435 shale of accretionary complex: Examples from the Shimanto Belt, southwestern Japan.
436 *Journal of Structural Geology*, **29**, 697-711.
- 437 Kohlstedt, D. L., Evans, B., Mackwell, S. J., 1995. Strength of the lithosphere: constraints
438 imposed by laboratory experiments. *Journal of Geophysical Research-Solid Earth*, **100**,
439 17587-17602.
- 440 Lindeque, A., de Wit, M.J., Ryberg, T., Weber, M., Chevallier, L., 2011. Deep crustal profile
441 across the southern Karoo basin and Beattie magnetic anomaly, South Africa: an integrated
442 interpretation with tectonic implications. *South African Journal of Geology*, **114**, 265-292.
- 443 Lock, B.E., 1980. Flat-plate subduction and the Cape Fold Belt of South Africa. *Geology*, **8**, 35-
444 39.
- 445 Mantero, E.M., Alonso-Chaves, F.M., Carcia-Navarro, E., Azor, A., 2011. Tectonic style and
446 structural analysis of the Puebla de Guzman Antiform (Iberian Pyrite Belt, South
447 Portuguese Zone, SW Spain). In J. Poblet and R.J. Lisle (Eds.), *Kinematic Evolution and*
448 *Structural Styles of Fold-and-Thrust Belts*. Geological Society, London, *Special*
449 *Publication*, **349**, 199-218.
- 450 McClay, K.R., 1977. Pressure solution and Coble creep in rocks and minerals. *Journal of the*
451 *Geological Society*, **134**, 57-70.
- 452 Mitra, S., 1990. Fault-propagation folds: geometry, kinematics and hydrocarbon traps. *AAPG*
453 *Bulletin*, **74**, 921-945.
- 454 Paton, D.A., 2006. Influence of crustal heterogeneity on normal fault dimensions and evolution:
455 southern South Africa extensional system. *Journal of Structural Geology*, **28**, 868-886.

- 456 Paton, D.A., Macdonald, D.I.M., Underhill, J.R., 2006. Applicability of thin or thick skinned
457 structural models in a region of multiple inversion episodes; southern South Africa.
458 *Journal of Structural Geology*, **28**, 1933-1947.
- 459 Pfiffner, O.A., Ramsay, J.G., 1982. Constraints on geological strain rates: arguments from finite
460 strain states of naturally deformed rocks. *Journal of Geophysical Research*, **87**, 311-321.
- 461 Rimstidt, J.D., 1997. Quartz solubility at low temperatures. *Geochimica et Cosmochimica Acta*,
462 **13**, 2553-2558.
- 463 Rutter, E. H., 1983. Pressure solution in nature, theory and experiment. *Journal of the*
464 *Geological Society of London*, **140**, 725-740.
- 465 Secor, D.T., 1965. Role of fluid pressure in jointing. *American Journal of Science*, **263**, 633-646.
- 466 Sibson, R.H., 1983. Continental fault structure and the shallow earthquake source. *Journal of the*
467 *Geological Society*, **140**, 741-767.
- 468 Suppe, J., 1983. Geometry and kinematics of fault-bend folding. *American Journal of Science*,
469 **283**, 684-721.
- 470 Tankard, A., Welsink, H., Aukes, P., Newton, R., Stettler, E., 2009. Tectonic evolution of the
471 Cape and Karoo basins of South Africa. *Marine and Petroleum Geology*, **26**, 1379-1412.
- 472 Visser, J.N.J., 1987. The influence of topography on the Permo-Carboniferous glaciation in the
473 Karoo Basin and adjoining areas, Southern Africa. In D.H. Elliot, J.W. Collison, G.D.
474 McKenzie and S.M. Haban (Editors), *Gondwana 6*, American Geophysical Union,
475 Washington, pp. 123-129.
- 476 Visser, J.N.J., 1997. Deglaciation sequences in the Permo-Carboniferous Karoo and Kalahari
477 basins of southern Africa: A tool in the analysis of cyclic glaciomarine basin fills.
478 *Sedimentology*, **44**, 507-521.

479 Visser, J.N.J., van Niekerk, B.N., van der Merwe, S.W., 1997. Sediment transport of the Late
480 Paleozoic glacial Dwyka Group in the southwestern Karoo Basin. *South African Journal of*
481 *Geology*, **100**, 223-236.

482 Yonkee, W.A, Czech, D.M., Nachbor, A.C., Barszewski, C., Pantone, S., Balgord, E.A.,
483 Johnson, K.R., 2013. Strain accumulation and fluid-rock interaction in a naturally
484 deformed diamictites, Willard thrust system, Utah (USA): Implications for crustal rheology
485 and strain softening. *Journal of Structural Geology*, **50**, 91-118.

486

487 **Figure captions**

488

489 **Figure 1:** a) Map showing simplified lithostratigraphy of the Cape Fold Belt and the location of
490 the study area near Laingsburg (after Paton *et al.*, 2006; Tankard *et al.*, 2009). The dashed line
491 shows the location of the Cape Fold Belt-Agulhas Bank Transect (Hälbich, 1993), on which the
492 cross-section in (b) is based. b) Cross-section illustrating the north-south variation in geometry
493 across the Cape Fold Belt (after Hälbich, 1993; Paton, 2006). The study area is along strike from
494 the northern end of this cross section, where the base of the Karoo Supergroup crops out, and
495 folding style changes from inclined to upright. c) Simplified cross-section of the study area,
496 illustrating the change in folding style from south to north.

497

498 **Figure 2:** Lower hemisphere, equal area stereoplots showing representative, regional fold limbs
499 (solid great circles) and axial planes (dashed great circle) in the (a) southern and (b) northern
500 parts of the study area. Note the change from moderately inclined to upright folding from south
501 to north, over a distance of approximately 10 km (c.f. Fig. 1c). (c) Poles to planes for cleavage in

502 Dwyka diamictite in the south (open circles) and north (filled circles), with dashed great circles
503 representing the average cleavage planes in the south and north of the study area. Note the
504 approximately axial planar orientation of the cleavage planes.

505

506 **Figure 3:** Field photographs of Dwyka diamictite. (a) Rare exposure of bedding in the Dwyka
507 Group (cycle 2c), defined by a subvertical boulder bed. The average plane of the anastomosing
508 cleavage dips about 45° to the south. (b) Well developed ‘tombstone’ cleavage in Dwyka (cycle
509 3c), further north than (a), and the cleavage is here steeply inclined. (c) Close up on subvertical
510 cleavage in Dwyka cycle 3c, where subhorizontal fractures (perpendicular to cleavage) can be
511 seen within a dropstone.

512

513 **Figure 4:** Logarithmic plot of longest dimension of largest contained dropstone against
514 ‘tombstone’ long axis length. The plot illustrates the qualitative observation that the size of
515 ‘tombstones’ of Dwyka, defined by preferential weathering along cleavage planes, is controlled
516 by the size of dropstones within the ‘tombstones’. This emphasizes that cleavage spacing is
517 controlled by dropstone size.

518

519 **Figure 5:** Photomicrographs in plane polarized light of cleavage seams in Dwyka Group
520 diamictites (all cycle 3c) cut perpendicular to cleavage. All the photographs are rotated such that
521 the average cleavage orientation is subhorizontal. (a) Relatively distributed cleavage, note
522 dissolved edges of quartz clasts (arrows), and the anastomosing nature of the, on average,
523 horizontal cleavage in this photomicrograph. (b) High cleavage density at the edge, and between
524 edges, of larger dropstones, again note the dissolved edges of quartz clasts (white arrows). (c)

525 Sealed tensile microfractures within a small dropstone. Note that the fractures are perpendicular
526 to cleavage in surrounding matrix (white arrows), indicating the fractures and cleavage formed in
527 the same stress field.

528
529 **Figure 6:** X-ray diffraction spectra of matrix material from a representative sample from each
530 cycle of the Dwyka diamictite exposed in the study area. Little variation is observed between the
531 different cycles, and the major minerals are quartz, feldspars (albite, anorthite, and microcline),
532 illite-muscovite, and chlorite, in all samples.

533
534 **Figure 7:** Electron backscatter (EBS) image and element maps of the area indicated by the white
535 rectangle on the photomicrograph (plane polarized light). On the element maps, warm colours
536 (red, yellow) represent high relative abundance, and cold colours (blue, black) relatively low
537 abundance. Cleavage seams stand out as bright on the EBS image, and are depleted in Si,
538 enriched in Al, K, and Fe. Scale bars are 100 μm long.

539
540 **Figure 8:** Electron backscatter (EBS) image and element maps of the area indicated by the white
541 rectangle on the photomicrograph (plane polarized light), an area of particularly dense solution
542 cleavage. On the element maps, warm colours (red, yellow) represent high relative abundance,
543 and cold colours (blue, black) relatively low abundance. Cleavage stands out as bright on the
544 EBS image, and is depleted in Si, enriched in Al, K, and Fe. Scale bars are 50 μm long.

545
546 **Figure 9:** Plot of strain rate (base 10 logarithm) against diffusive distance d calculated for a
547 pressure solution flow law assuming diffusion as the rate-limiting process (Gratier et al., 2009).

Å. Fagereng: Pressure solution cleavage in Dwyka diamictite

548 The plot is contoured for temperature, and a shaded area shows typical cleavage spacing (and
549 grain size) in the Dwyka Group diamictite.

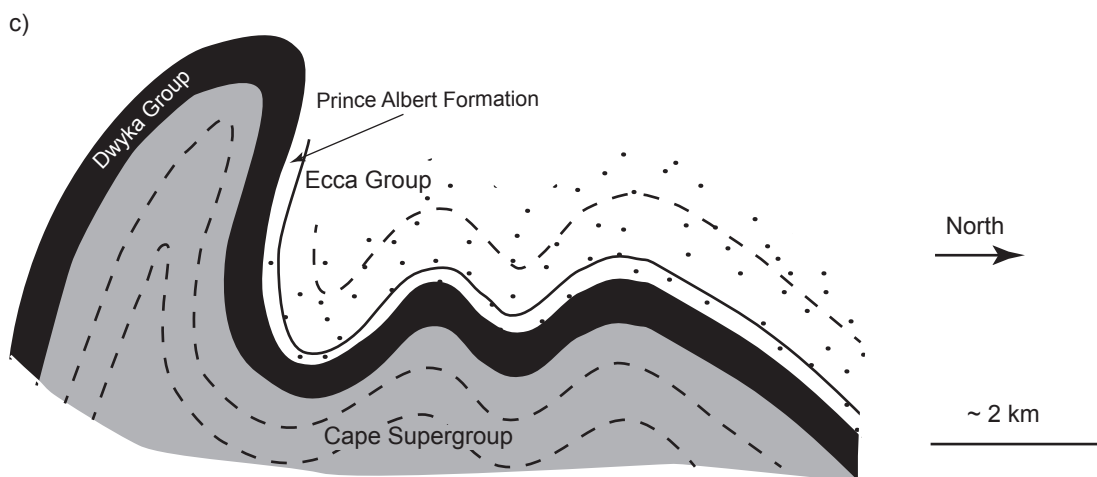
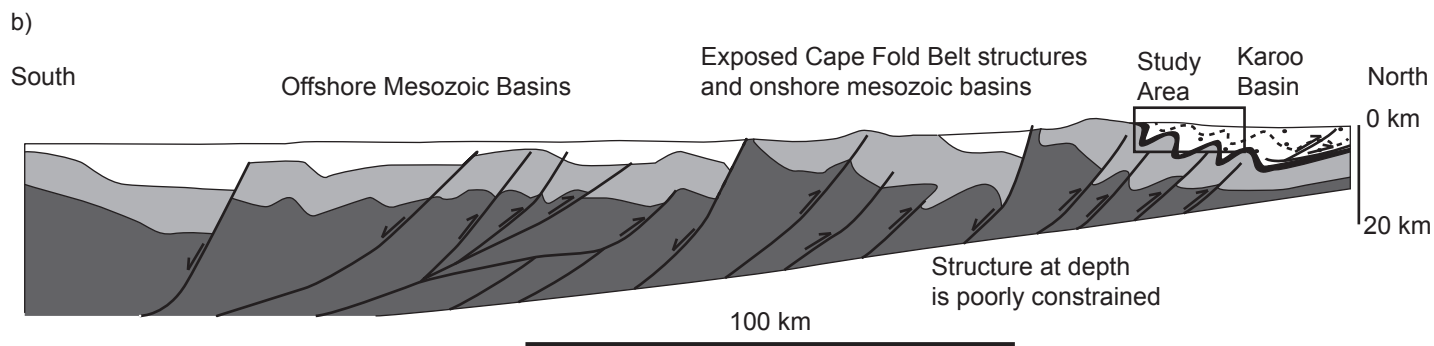
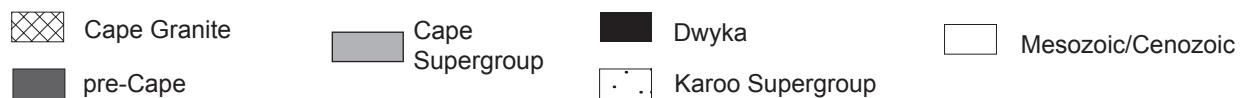
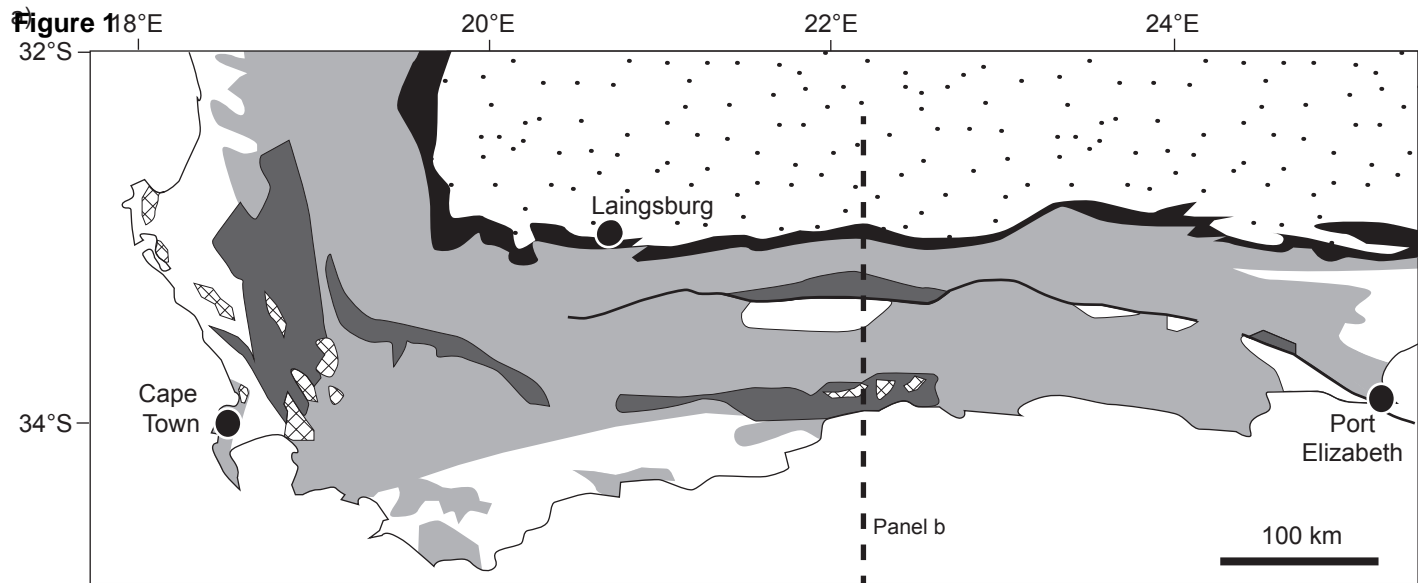
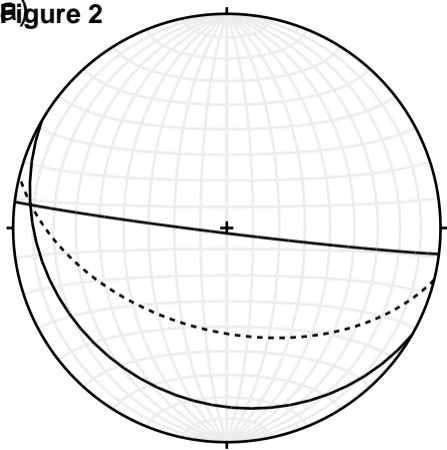
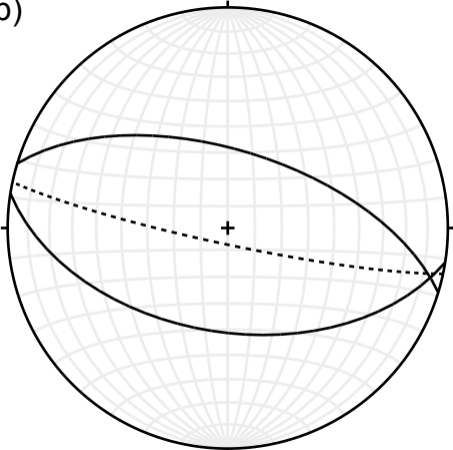


Figure 2



b)



c)

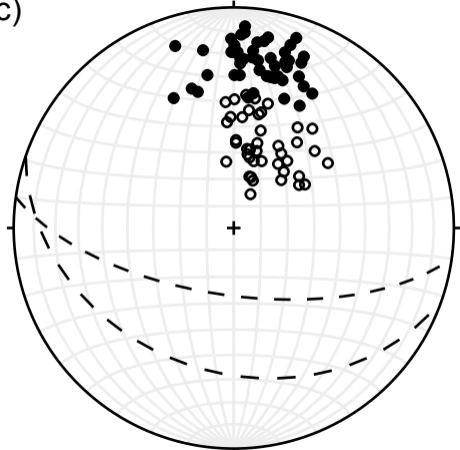


Figure 3



Figure 4

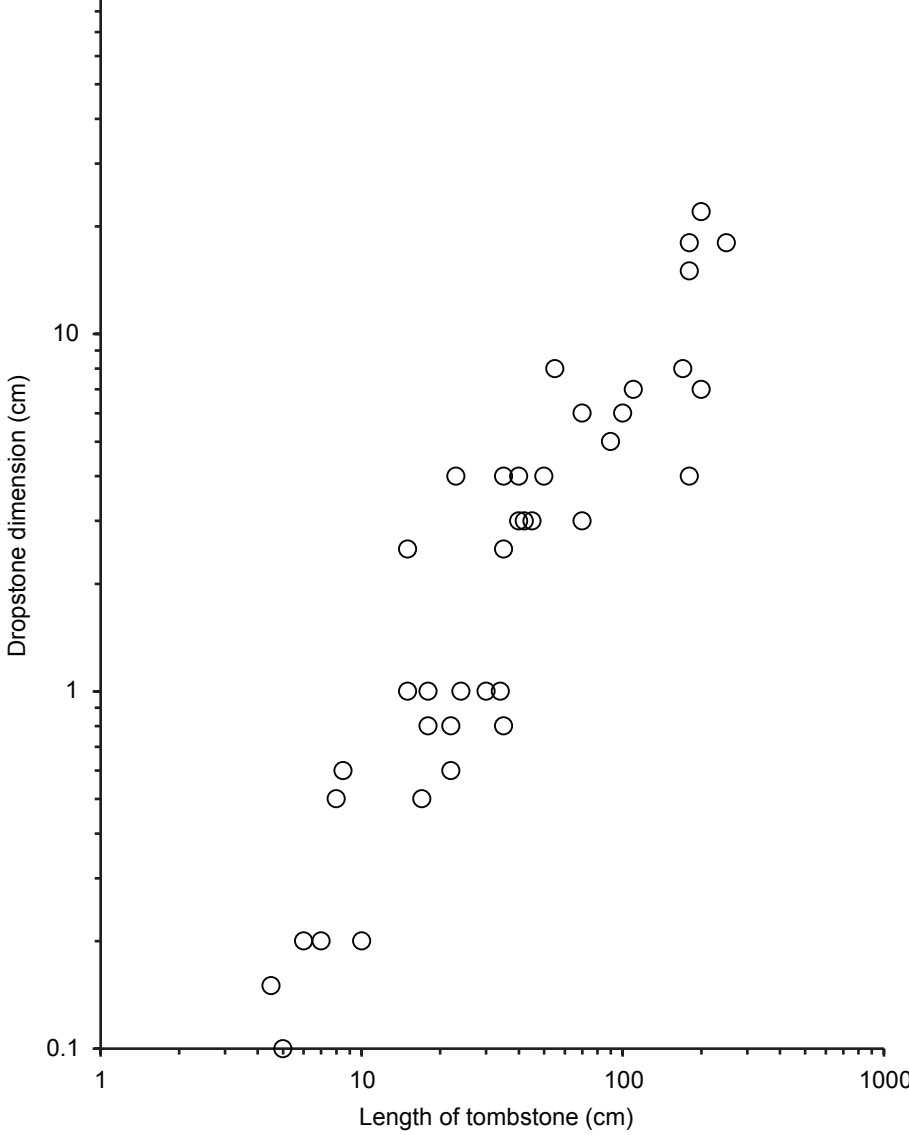


Figure 5

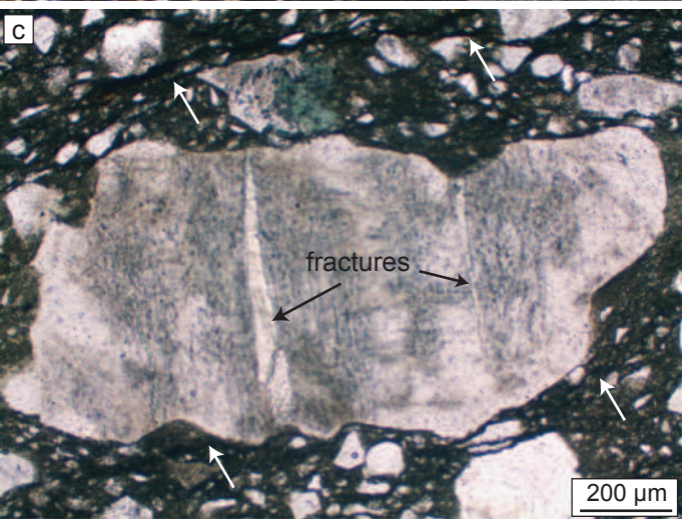
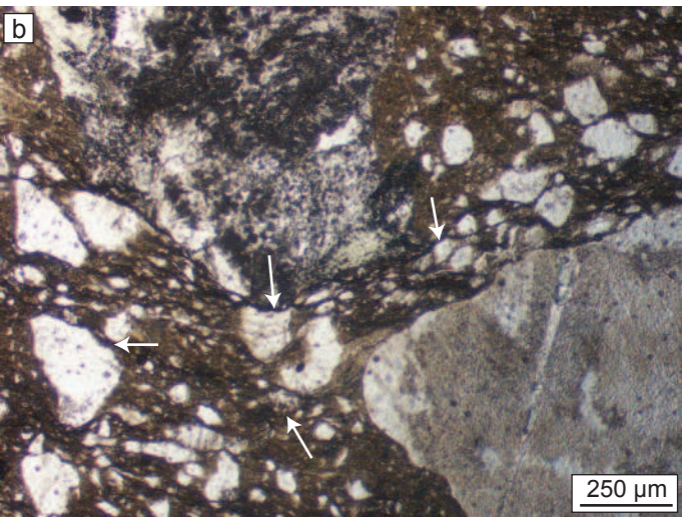
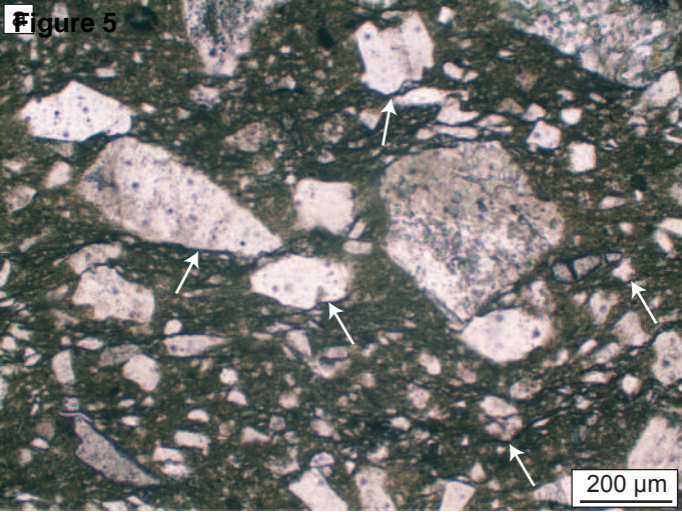


Figure 6

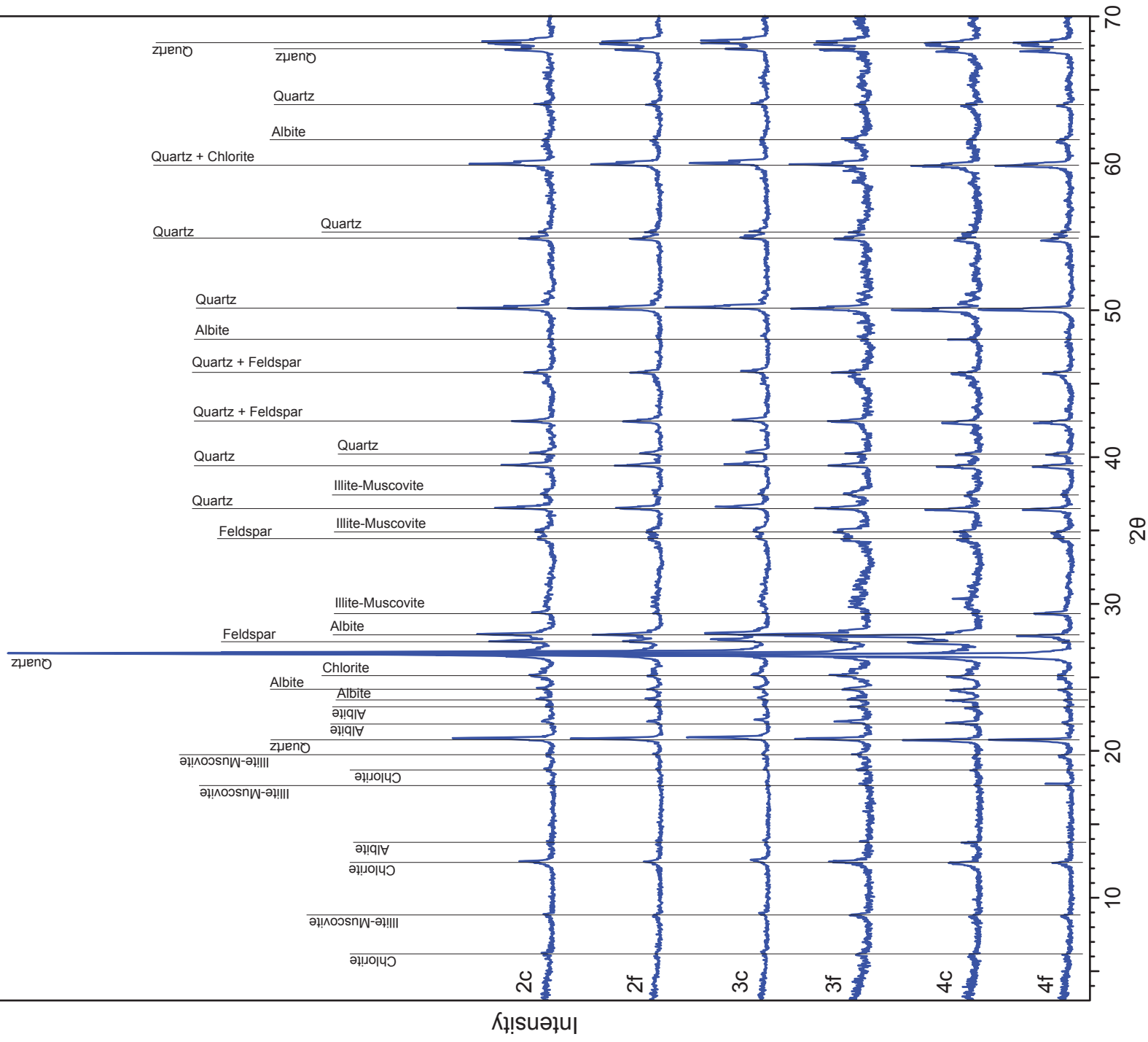


Figure 7

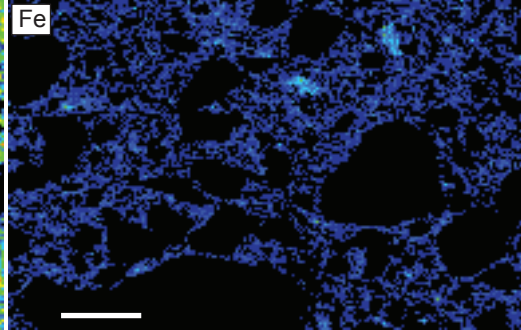
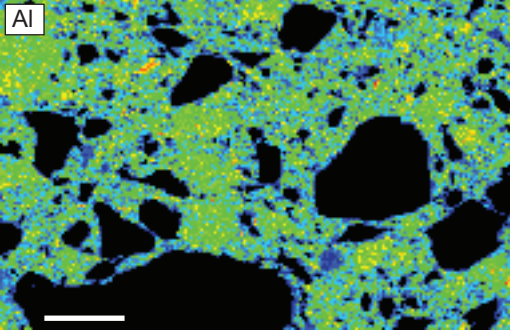
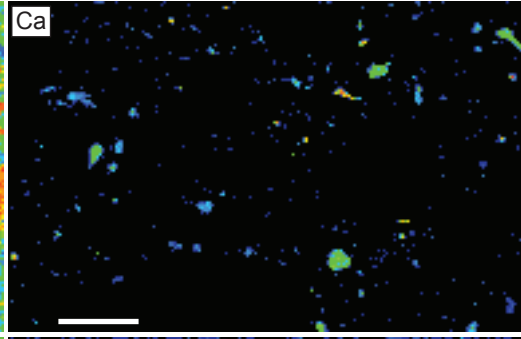
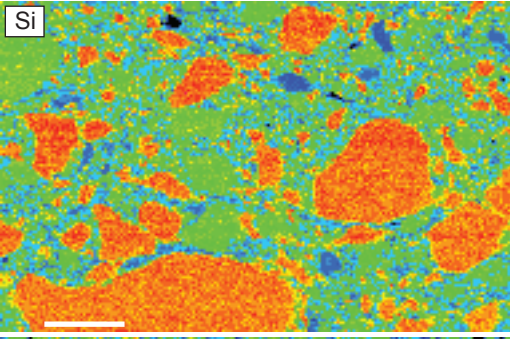
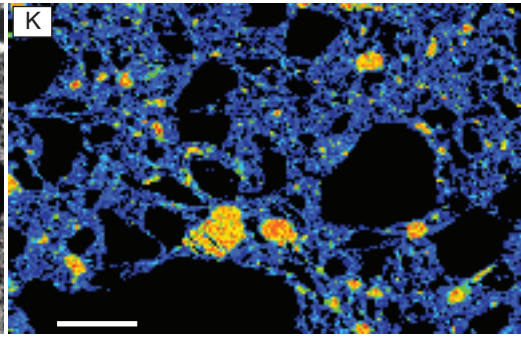
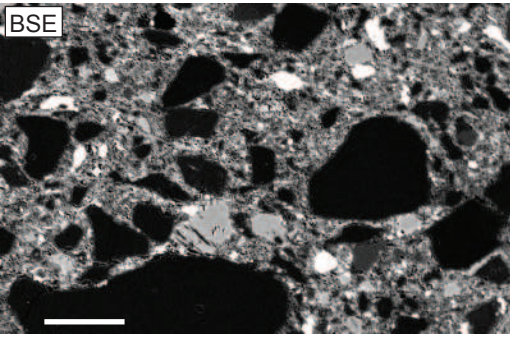
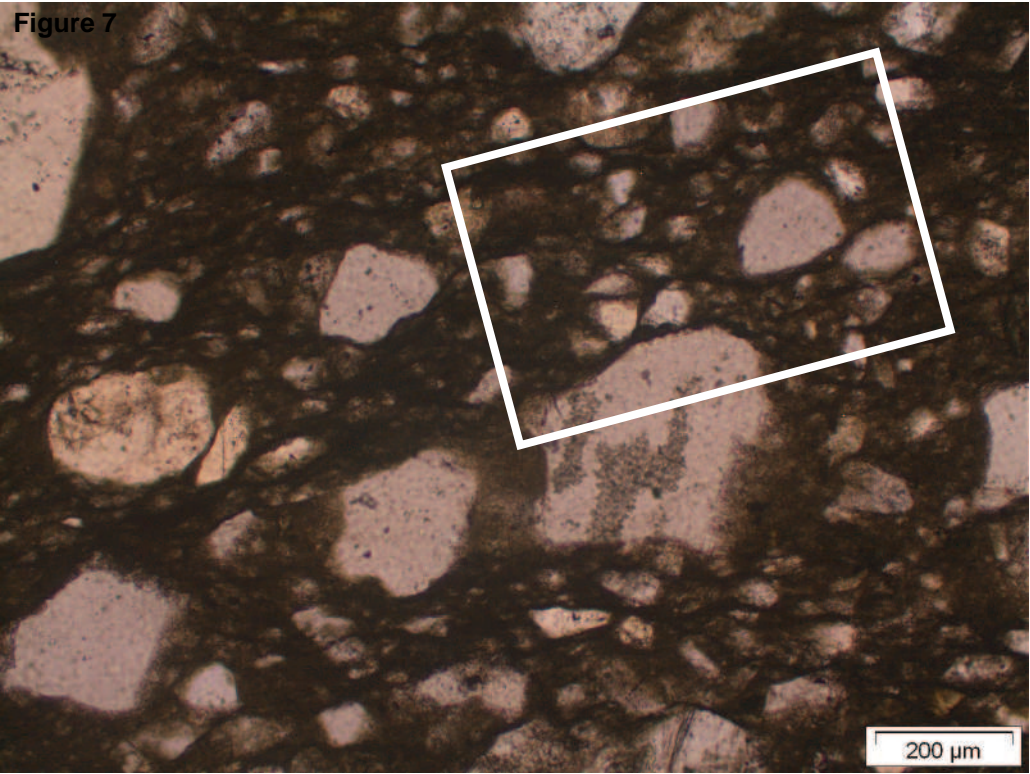


Figure 8

